
14 Aug 2019

Frequency Domain Measurements of Melt Pool Recoil Pressure using Modal Analysis and Prospects for In-Situ Non-Destructive Testing

Tristan Cullom

Nicholas Altese

Douglas A. Bristow

Missouri University of Science and Technology, dbristow@mst.edu

Robert G. Landers

Missouri University of Science and Technology, landersr@mst.edu

et. al. For a complete list of authors, see https://scholarsmine.mst.edu/mec_aereng_facwork/4726

Follow this and additional works at: https://scholarsmine.mst.edu/mec_aereng_facwork



Part of the [Manufacturing Commons](#)

Recommended Citation

T. Cullom and N. Altese and D. A. Bristow and R. G. Landers and B. Brown and T. Hartwig and D. Soine and A. Allen and A. Barnard and J. Blough and K. Johnson and E. C. Kinzel, "Frequency Domain Measurements of Melt Pool Recoil Pressure using Modal Analysis and Prospects for In-Situ Non-Destructive Testing," *Proceedings of the 30th Annual International Solid Freeform Fabrication Symposium (2019, Austin, TX)*, pp. 1430-1444, University of Texas at Austin, Aug 2019.

This Article - Conference proceedings is brought to you for free and open access by Scholars' Mine. It has been accepted for inclusion in Mechanical and Aerospace Engineering Faculty Research & Creative Works by an authorized administrator of Scholars' Mine. This work is protected by U. S. Copyright Law. Unauthorized use including reproduction for redistribution requires the permission of the copyright holder. For more information, please contact scholarsmine@mst.edu.

Frequency Domain Measurements of Melt Pool Recoil Pressure Using Modal Analysis and Prospects for In-Situ Non-Destructive Testing

Tristan Cullom¹, Nicholas Altese¹, Douglas Bristow¹, Robert Landers¹
Ben Brown², Troy Hartwig², David Soine²
Aimee Allen³, Andrew Barnard³, Jason Blough³, Kevin Johnson³
Edward Kinzel⁴

¹Department of Mechanical and Aerospace Engineering, Missouri University of Science and
Technology, Rolla, MO 65409.

²Department of Energy's Kansas City National Security Campus, Kansas City, MO 64147.

³Department of Mechanical Engineering – Engineering Mechanics, Michigan Technological
University, Houghton, MI 49931.

⁴Department of Aerospace and Mechanical Engineering, University of Notre Dame, Notre Dame,
IN 46556

Department of Energy's Kansas City National Security Campus which is operated and managed
by Honeywell Federal Manufacturing Technologies, LLC under contract number DE-
NA0002839.

Abstract

Fielding Additively Manufactured (AM) parts requires evaluating both the part's geometry and material state. This includes geometry that may be optically hidden. Both the geometry and material state affect the vibration response of the parts and modal analysis (identifying natural frequencies) has been shown to be effective for at least simple geometries using ex-situ methods (shaker table and impact hammer excitations). This paper investigates evaluation of the frequency response of metal parts inside the build chamber using the process laser to excite the parts during printing (Renishaw AM250). Vibrations in the part are measured with accelerometers connected to the build plates and used to track the response during printing as during pauses between layers. The laser is modulated at different frequencies and focused onto specific targets to precisely extract the response from individual parts on the build plate. These results are compared to numerical models for metal parts of different geometries and with different material states. This work was funded by the Department of Energy's Kansas City National Security Campus which is operated and managed by Honeywell Federal Manufacturing Technologies, LLC under contract number DE-NA0002839.

1. Introduction

Additive manufacturing is a growing means of producing parts due to its ability to create complex geometries that would otherwise be impossible to make with traditional methods. With the need for quality assurance being critical, evaluation of parts that are produced is an on-going field of study in the additive community. Evaluation schemes in the form of both destructive and non-destructive methodologies are the subject of research for both in and ex-situ analysis of these additively manufactured parts. Selective Laser Melting (SLM) is a common means of additively manufacturing metal parts; the range of materials that can be produced from SLM range from stainless steels, titanium, aluminum, nickel alloys, and composites. With each material that is produced, one of the direst concerns is that of porosity, which can affect the quality and performance of the parts that are produced.

The SLM process starts with a thin layer of powder that is spread over a build substrate at which point a focused laser scans over a pre-defined part geometry. The interaction between the laser and the layer of powder is a complex thermal process. The energy from the laser is absorbed into the layer via conduction and advection, resulting in fusion between the powder layer and substrate. The quality of this fusion is dependent on a key factor: recoil pressure; the origin of recoil pressure is due to the vaporization of the surface of the melt pool. With both the recoil pressure and Marangoni convection, the dynamics of the melt pool are described. Semek et al. reported that the vaporization-induced recoil pressure induces the ejection of the melt pool to form spatter [2]. [3] observed that the oscillations of recoil pressure resulted in the fluctuations observed in the formation of the rear keyhole wall. Using multi-laser technology, M. T. Andani et al was able to observe that with the increase in recoil pressure generated by multiple lasers, the amount of metallic material ejected from the melt pool is also increased [4]. [5] was able to experimentally observe the development in the melt pool using high-speed x-ray imaging and correlate it to the recoil pressure at that instant in time.

In addition to experimental observations, various studies have been conducted in order to model and experimentally quantify the recoil pressure at the melt pool [6-8]. Simulating the interaction between the laser and powder bed involves incorporating both the thermal and dynamic interaction at the powder bed. Numerical simulations employ recoil pressure models that are based on the Clausius-Clapeyron model in order to better estimate how the recoil pressure influences metrics such as spatter ejection speed and temperature gradients at the melt pool [6,7]. As additional merit, [6] compared the ejection speeds of the particles in the simulation with experimental results using high-speed imaging and found that the behavior of both instances closely matched. By modeling the recoil pressure with this model, the behavior of the spatter and melt pool was able to be accurately described. C. Zhao et al. were able to observe changes in the spatter and correlated it to changes in the recoil pressure exerted on the melt pool [8]. This study estimated the recoil pressure in observation from literature by applying both the Clausius-Clapeyron model and assuming the pressure exerted onto the ejected spatter was directly related to the recoil pressure; the order of magnitude for the recoil pressure estimations was on the order of 60 kPa. This pressure can be made to be an equivalent force by multiplying by the average spot size diameter of the laser, in this case, 70 μm , which yields an equivalent force on the order

of 0.25 mN. The ability to measure the magnitude of the estimated recoil pressure is not difficult but rather the ability to measure the pressure over an area as small as the melt pool proves to be quite difficult.

With recoil pressure being critical to the printing process, the ability to measure the pressure in-situ would allow real-time health monitoring of the melt pool. The ability to measure this pressure however, is difficult since the pressure is acting over a very small area. To calculate the recoil pressure, this study utilizes the frequency domain to calculation rather than temporal domain. The dynamics of the system given the force input from the laser shall be utilized from a modulated laser; the results from the measurements can then be extended to the Structural Health Monitoring (SHM) framework for NDT analysis of both the melt pool and parts that can be printed.

2. AM250 Dynamics

The Renishaw AM250 additive manufacturing system utilizes an Acousto-Optic Modulator (AOM). This modulation allows for the control of the laser's Pulse Repetition Frequency (PRF) through changes in the intensity of the sound wave that is diffracting the laser; this behavior is utilized for the purpose of being able to further control the melt pool. To understand the shape and periodicity of the waveform, a sample pulse mode was recorded using an experimental set-up involving a photodetector with a bandpass filter. The schematic of the experimental set-up, the same pulse mode, as well as the pulse mode in the frequency domain can be seen in Figure 1.

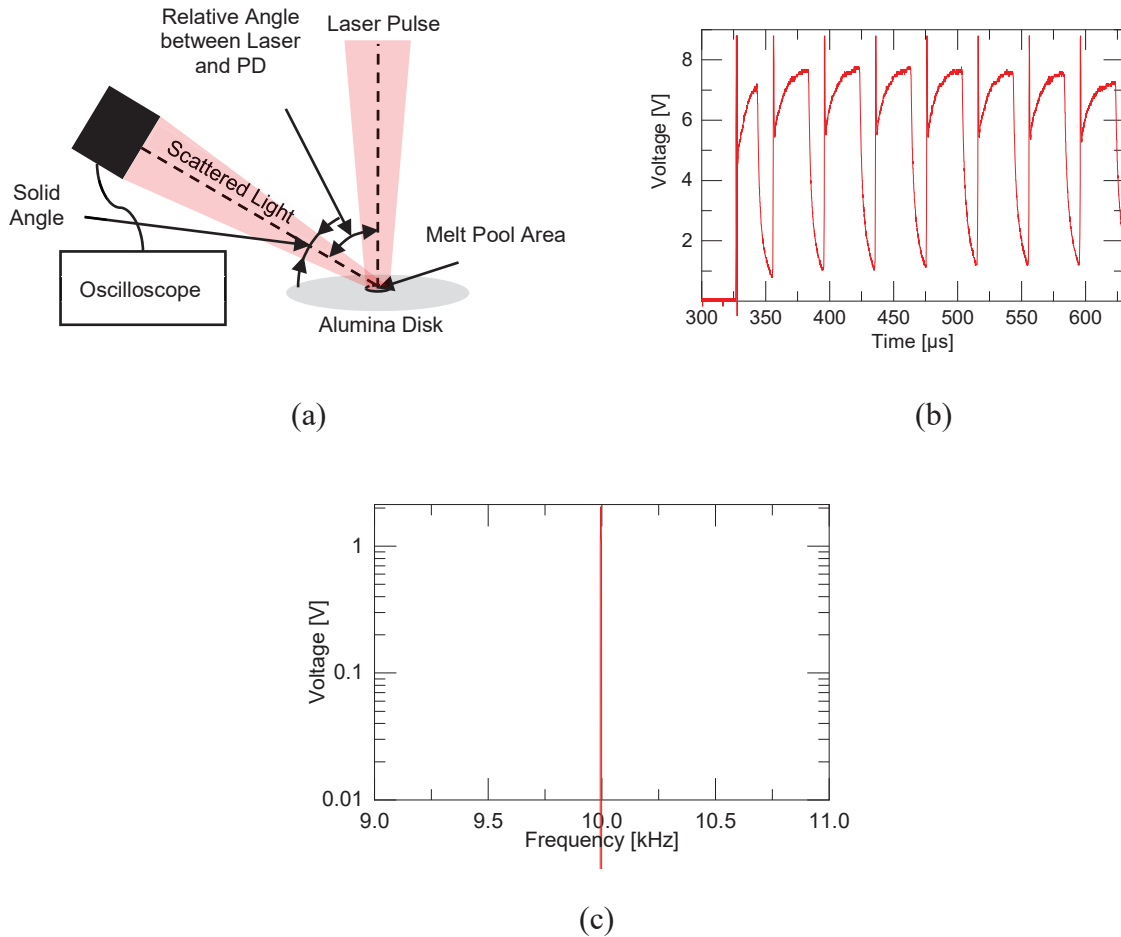


Figure 1: (a) Schematic of scattered light collection set-up (b) sample pulse mode

Figure 1a shows the schematic in which the pulse mode was measured by incorporating a PDA100A2 photodetector and an oscilloscope. The radiance from the laser was collected by scattering it from an alumina disk. Figure 1b is an example of a pulse mode for a given set of processing parameters and Figure 1c is the Fourier-Transform of the pulse mode. Modulating the laser allows for the laser to drive the part at a specific frequency and as a result, be able to record the response from the part and by extension, calculate the force and recoil pressure from the laser.

3. Modeling Interaction Between Laser and Printed Part

To model the interaction between a part that has been printed and the laser, a simple Single Degree of Freedom (SDOF) mass-spring-damper model in which the forcing function was modeled as the laser, which can be seen below in Figure 2.

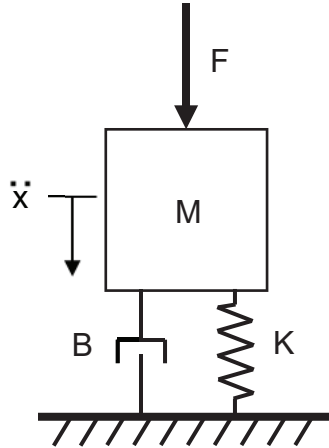


Figure 2: SDOF model used to model interaction between laser and part.

The equation of motion of Figure 1 is,

$$M\ddot{x} + B\dot{x} + Kx = F \quad (1)$$

Where M , B , and K represent the mass, damping, and stiffness of the part and F is the forcing function due to the laser. For simplicity, the steady-state behavior of the system was found and transients were ignored. The canonical form of (1) was found by dividing (1) by M which yields,

$$\ddot{x} + 2\zeta\omega_n\dot{x} + \omega_n^2x = \frac{\omega_n^2F(t)}{K} \quad (2)$$

Assuming that the forcing function is of the form $F(t) = F_o \sin \omega t$ and that the solution of the system is of the form $x(t) = X \sin(\omega t)$, (2) yields the steady-state form of the position of the system,

$$X = \frac{F_o e^{-j\phi}}{K\sqrt{(1-r^2)^2 + 4\zeta^2r^2}} \quad (3)$$

Where,

$$r = \frac{\omega}{\omega_n}$$

$$\phi = \begin{cases} \tan^{-1}\left(\frac{2\zeta r}{1-r^2}\right) & \text{for } r \leq 1 \\ \pi - \tan^{-1}\left(\frac{2\zeta r}{r^2-1}\right) & \text{for } r > 1 \end{cases}$$

Plugging these values into the steady-state solution yields,

$$\ddot{x}(t) = \frac{F_o \sin(\omega t - \phi)}{K \sqrt{(1-r^2)^2 + 4\zeta^2 r^2}} \quad (4)$$

At this point, the magnitude of the forcing function is required in order to model the dynamics of the system in steady-state. The magnitude of the force was calculated by assuming that the energy from the laser was able to be converted into the kinetic energy of the melt pool, which can be seen below,

$$P_{laser} t_{laser,on} e^{-\zeta_{laser} t_{laser,on}} = \frac{1}{2} m_{melt\ pool} v_{melt\ pool}^2 \quad (5)$$

Where P is the laser power, t is the period in which the laser is on, m is the approximate mass of the melt pool and ζ is the damping ratio of the laser. The purpose of the damping ratio is to have a negative rate of change in the kinetic energy of the system. Taking the derivative of (5) with respect to the time that the laser is on and then multiplying by the mass of the mass pool yields the approximate force magnitude that would be exerted onto the melt pool,

$$F_o(t_{laser,on}) = \frac{m_{melt\ pool} P_{laser} e^{-\zeta_{laser} t_{laser,on}} (1 - t_{laser,on} \zeta_{laser})}{\sqrt{2 P_{laser} t_{laser,on} m_{melt\ pool} e^{-\zeta_{laser} t_{laser,on}}}} \quad (6)$$

(6) is then plugged into (4), and then the double derivative with respect to time to calculate the acceleration of the part, yielding,

$$\ddot{x}(t) = \frac{-\omega^2 F_o \sin(\omega t - \phi)}{K \sqrt{(1-r^2)^2 + 4\zeta_{part}^2 r^2}} \quad (7)$$

With (7), the ratio between the laser frequency and part frequency yields a maximum response when the part is driven near its natural frequency. For NDT purposes, the response from the part when driven by a laser can be indicative of the recoil pressure as it is being printed.

4. Experimental Theory

The relationship between the FRF, acceleration, and force is,

$$FRF(f) = \frac{a(f)}{F(f)} \quad (8)$$

From (8), if the acceleration of a part as well as the FRF is known, the forcing function that would be exerted onto the part can be calculated. An example of an FRF can be seen with a simple tuning fork; an ANSYS simulation was conducted in which the tip of the prong was excited by a 1 N force and the acceleration in the same direction as the force was measured. The FRF from the tuning fork can be seen in Figure 3 below.

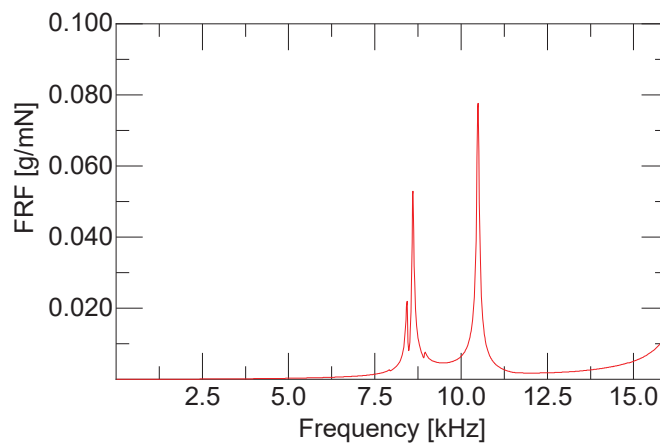


Figure 3: FRF from tuning fork from ANSYS simulation.

With Figure 3 the response of the part at resonance is several orders of magnitude higher than off-resonance. With this tuning fork, the FRF is indicative of the part's sensitivity to an input force at a range of frequencies. By leveraging the part near resonance, the acceleration that would be measured would be maximized.

5. Experimental Set-Up

A build was created in which four sets of tuning forks were printed that were designed to resonate at a frequency: 4, 6, 8, and 10 kHz. Three copies of each frequency tuning fork were printed, and they were arranged in rows, with Figure 4 showing a view of the build, with a number designation being seen in the figure to represent the frequencies of the tuning forks as well as the one that was excited being inscribed with a circle.



Figure 4: Picture of tuning fork build for excitation experiment.

Prior to being excited by the laser, an impact test was conducted on the 10 kHz tuning fork seen in Figure 4 for the purpose of seeing its first resonate frequency as well as having the FRF for the purpose of calculating the forcing spectrum; the FRF can be seen in Figure 5. With respect to the coupling of energy between the part's acceleration and the location of the accelerometer, an ANSYS simulation was ran in which the magnitude of acceleration was measured with a 1 N force input was measured at the same location as the force input and the same location as what is seen in Figure 4, with the ANSYS simulation results being seen in Figure 6.

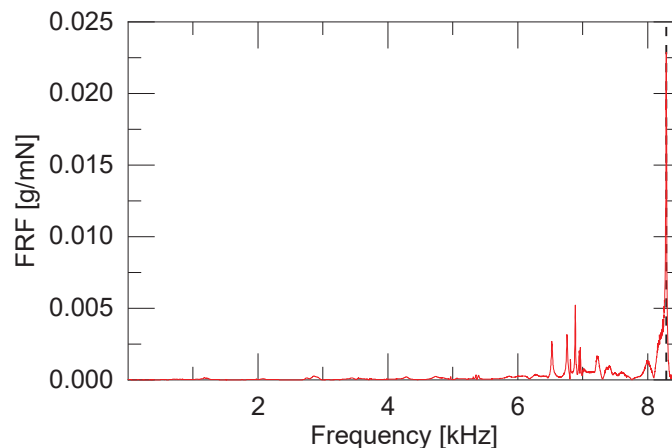


Figure 5: Experimental FRF of 10 kHz tuning fork.

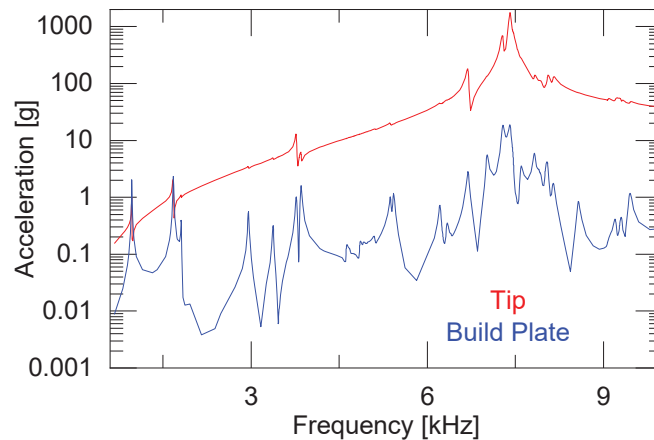


Figure 6: ANSYS FRF comparison when response from tuning fork was measured at tuning fork tip and build plate.

From Figure 5, experimentally, FRFs are not as clean as a simulation would suggest. The first mode of the tuning fork that would later be excited occurred at 8.288 kHz, seen by the vertical peak in the graph. With respect to the magnitude that would be measured by the accelerometer, an ANSYS simulation was conducted in which measurements were taken at the point of contact of the force and the location on the build plate where the accelerometer was placed for the experimental FRF. Figure 6 showcases the significant difference in magnitude at the first mode of the structure. For experimental purposes, placing the accelerometer on the build plate rather than the part itself serves two purposes: protecting the accelerometer from successive laser pulses and being able to monitor more than one part. For NDT testing, this placement of the accelerometer allows for continuous monitoring of parts as they are printing.

For the excitation scheme, PRFs were selected based on being banded around the first mode of the tuning fork: 8.288 kHz. Given that the resolution of the AM250 for PRF variance is on the order of 10 μ s, the PRFs that were able to be generated were 7.1, 7.7, 8.3, 9.1, and 10 kHz. For each PRF pulse, data was collected from the accelerometer using a NI 9234 DAQ that sampled at 51.2 kHz.

6. Experimental Results

The acceleration spectrums that were measured for each PRF was compared against each other in Figure 7. The frequency band of interest was centered about resonance of the part with the closest PRF, 8.3 kHz, is seen as a vertical dashed line in the graph.

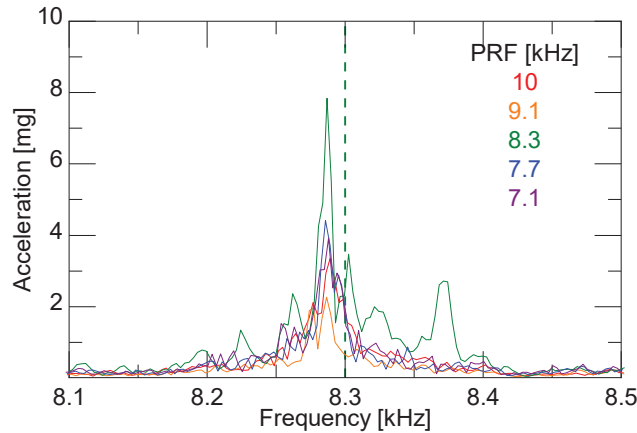


Figure 7: Measured acceleration spectrums for various PRFs.

For the five PRFs, the maximum acceleration that was measured was 8 mg. The PRF that corresponded to this acceleration was the 8.3 kHz PRF. This is due to the laser's frequency being close to that of the parts, resulting in the acceleration being maximized. With each acceleration spectrum, Eq. 8 was used and the forcing spectrum was calculated by dividing acceleration spectrums by the experimental FRF of the tuning fork; the resulting forcing spectrums can be seen in Figure 8.

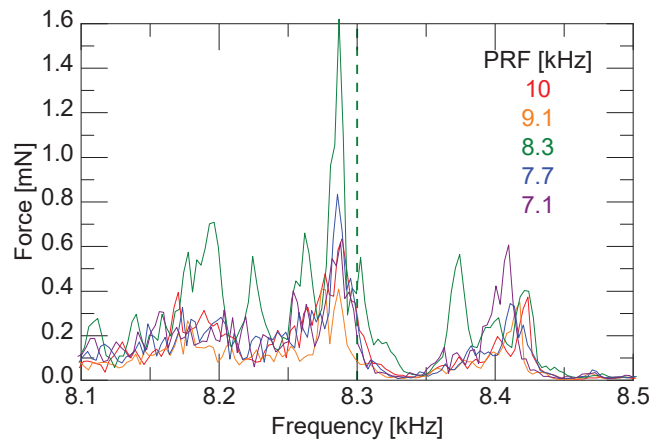


Figure 8: Calculated forcing spectrums for various PRFs.

The maximum force that was measured was 1.62 mN at resonance. Like the acceleration spectrum, this magnitude occurred when the PRF was closest to resonance. To relate the force measurement in Figure 8 to the recoil pressure, an average area of the spot size of the laser was used as the cross-sectional area of the applied force: 75 μm . The equivalent pressure was calculated to be 360 kPa. With the estimations from the literature that were calculated from this study being on the order of 60 kPa, the measured force and equivalent recoil pressure are on the same order of magnitude as estimations.

7. Uncertainty in Measurements

To investigate the confidence in the magnitudes in both the force and recoil pressure, propagation of uncertainty was calculated. The uncertainty of the force was calculated first using the relationship between force, acceleration, and the FRF of the structure,

$$\sigma_{force}(f) = \sqrt{\frac{\sigma_{laser}^2(f)}{FRF^2(f)} + \frac{a_{laser}^2(f)\sigma_{FRF}^2(f)}{FRF^4(f)}} \quad (9)$$

The uncertainty in the force was plotted with the frequency band centered around the resonance of the tuning fork below. The summation of both terms in (9) was compared to just the first term based on looking into the difference in magnitude at resonance; both spectrums were plotted and can be seen in Figure 10 below for one of the PRFs as a means of behavior comparison rather than magnitude; the uncertainty spectrum can be seen in Figure 9.

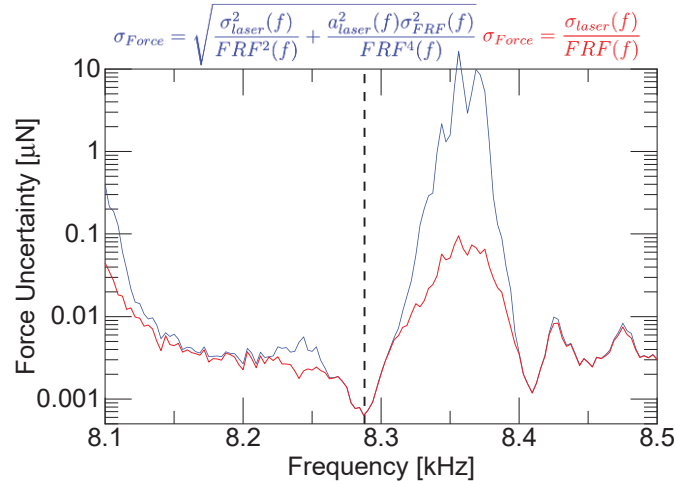


Figure 9: Uncertainty of force comparison at resonance between laser excitation and FRF components.

At resonance, the uncertainty is proportional to the FRF of the structure: the magnitude of uncertainty is lowest at the part's resonance. With this, the level of uncertainty can be minimized by driving the parts near resonance with the laser. The uncertainty spectrums were calculated for each PRF and were plotted about resonance and can be seen in Figure 10.

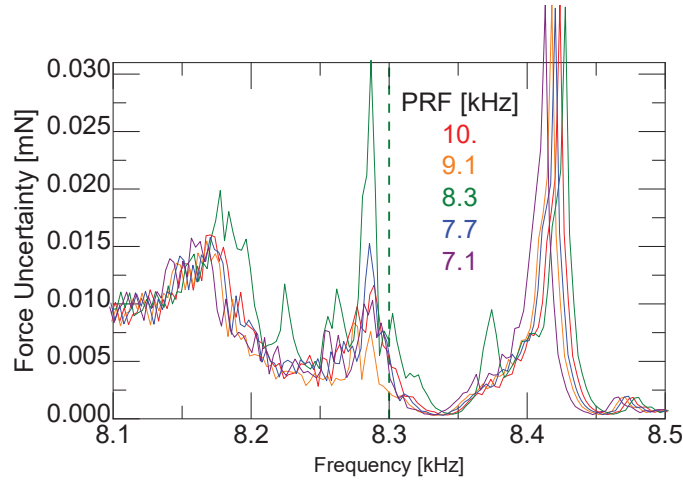


Figure 10: Force uncertainty spectrum for various PRFs.

The magnitude of uncertainty when the PRF is closest to resonance is $31 \mu\text{N}$. Since the magnitude of uncertainty scales with the FRF, the magnitude of uncertainty will always be largest with the PRF that is closest to resonance. The uncertainty in the recoil pressure was calculated by using a range of melt pool diameters from 50 to $100 \mu\text{m}$, yielding a standard deviation of $25 \mu\text{m}$ with the average melt pool diameter used be $75 \mu\text{m}$. The propagation of uncertainty illustrated with Eq. 9, the uncertainty for the recoil pressure was calculated for the 8.3 kHz PRF,

$$\sigma_{\text{Recoil Pressure}} = |P_{\text{Recoil}}| \sqrt{\left(\frac{\sigma_{\text{force}}}{F}\right)^2 + \left(\frac{\sigma_{\text{area}}}{A}\right)^2} \quad (10)$$

With Eq. 10, the uncertainty in the recoil pressure was calculated to be 41.3 kPa , leading to the recoil pressure at resonance for the closest PRF to be $360 \pm 41.3 \text{ kPa}$. This recoil pressure is on the same order of magnitude as previous literature that dealt with quantifying and modeling the recoil pressure during the printing process.

8. Discussion and Conclusions

The forcing function at resonance was calculated to be 1.62 ± 0.031 mN with the corresponding recoil pressure assuming variations in the melt pool diameter was calculated to be 360 ± 41.3 kPa. With literature estimations being on the order of 60 kPa, the equivalent force that would be expected to be measured is on the order of 1.1 mN. The force and pressure calculations from this experiment are on the same order of magnitude as the estimations from literature. The absolute difference in magnitudes can be attributed to the structure that was used for excitation as well as the way the part was excited with the laser.

With scope of this paper being NDT, a method for comparison is Acoustic Emission (AE). AE is a phenomenon that occurs when acoustic waves propagate through a medium when a solid undergoes a change in its internal structure; this can be seen to occur during the printing process as parts are formed at each layer. Studies have been able to observe changes in the acoustic signature of parts in both in and ex-situ circumstances [9-12]. L. W. Koester et al was able to differentiate between acoustic signatures with varying processing parameters in-situ during the SLM process [9]. The findings were able to be hypothesized to be able to correlate changes in the acoustic signature to defects that could potentially form during the printing process. [10-12] focused on ex-situ studies pertaining to the fatigue behavior of parts that were printed both additively and traditionally. [10,11] were able to observe a co-linear behavior between the acoustic signature measured and the growth of a crack in various types of metal plates. M. Strantza et al was able to observe an increase in the number of acoustic events, acoustic signals that go above a user-defined value, when the size of the crack maximized before failure. With AE testing, the ability to monitor parts as they are printing can allow for diagnosis to be performed to determine if a part is fine or needs to be stopped due to a crack starting to form.

Utilizing modal analysis for the purpose of a diagnostic method with laser excitation has good results about being able to quantify the recoil pressure. This is a simple extension of AE testing given that the structural response of a part will be measured during the printing process. It is not limited to measuring signals however, as it can be employed to the Structural Health Monitoring (SHM) framework by estimating the health of both the part and melt pool. The health of the part be estimations to the mass, stiffness, and damping matrices that describe the part layer-to-layer. By being able to measure the forcing function of the laser and tracking the acceleration, the model matrices of the part can be calculated and compared to a baseline as well as correlating changes in the melt pool's dynamics to transient changes in the magnitude of the recoil pressure.

9. Acknowledgements

This work was funded by the Department of Energy's Kansas City National Security Campus which is operated and managed by Honeywell Federal Manufacturing Technologies, LLC under contract number DE-NA0002839.

References

- [1] M. J. Matthews et al., “Denudation of metal powder layers in laser powder bed fusion processes.” *Acta Materialia*. 114. 33-42. (2016).
- [2] V. Semak et al., “The role of recoil pressure in energy balance during laser materials processing.”, *Journal of Physics D: Applied Physics*. 30. 2541–2552. (1997).
- [3] M. J. Zhang et al., “Observation of spatter formation mechanisms in high-power fiber laser welding of thick plate.” *Applied Surface Science*. 280. 868-875. (2013).
- [4] M. T. Andani et al., “Spatter formation in selective laser melting process using multi-laser technology.” *Materials and Design*. 131. 460-469. (2017).
- [5] C. Zhao et al., “Real-time monitoring of laser powder bed fusion process using high-speed X-ray imaging and diffraction.” *Scientific Reports*. 7. 3062. (2017).
- [6] S. Ly. et al., “Metal vapor micro-jet controls material redistribution in laser powder bed fusion additive manufacturing.” *Scientific Reports*. 7. 4085. (2017).
- [7] K.Q. Le et al., “On the study of keyhole-mode melting in selective laser melting process.” *International Journal of Thermal Sciences*. 145. 105992. (2019).
- [8] C. Zhao et al., “Bulk-explosion-induced metal spattering during laser processing.” *American Physical Society*. 9. 021052. (2019).
- [9] L. W. Koester et al., “In-situ acoustic signature monitoring in additive manufacturing processes.” *Proceedings of the 44th annual AIP conference*. (2018).
- [10] T. M. Roberts et al., “Acoustic emission monitoring of fatigue crack propagation.” *Journal of Constructional Steel Research*. 59. 695-712. (2003).
- [11] D. G. Aggelis et al., “Acoustic emission for fatigue damage characterization in metal plates.” *Mechanics Research Communications*. 38. 106-110. (2011).
- [12] M. Strantza et al., “Evaluation of SHM system produced by additive manufacturing via acoustic emission and other NDT methods.” *Sensors*. 15. 26709-26725. (2015).